HXR spectroscopy

Data Analysis Report M2 IRT
2021-2022

Written by David Paipa *
Presented to Dr. Nicole vilmer †

December 28, 2021
PSL — Observatoire de Paris

*. SUTS M2 IRT 2020-2021 . PSL - Obsevatoire de Paris. Meudon, France
†LESIA, Observatoire de Paris. 5 place Jules Janssen 92190. Meudon, France

Contents

1 Development **3**
1.1 "Quick-look" time profiles 3

2 Comparison of the count rates for different detectors **4**

3 Comparison of the count rates for different pixels **5**

4 Spectroscopy **6**

1 Development

On the following work I will present the assignment for the MC Data analysis on the topic HXR spectroscopy. The studied data if from STIX, the hard x-ray instrument onboard the Solar Orbiter, used to observe solar flares over a wide range of flare sizes.

1.1 "Quick-look" time profiles

A time profile of the count rates is made for each one of the 4 energy bands and displayed in figure 1. A micro solar flare is detected around 21h39m and a relevant increase in the counts is observed in the 4-10 KeV and 10-15 KeV bands, while for the 15-25 KeV band the S/N ratio is too small to consider it a event. The 25-50 KeV band shows no relevant response for this event. We can say that the 10-15 KeV band is the highest energy band for which the signal of the event is still relevant.

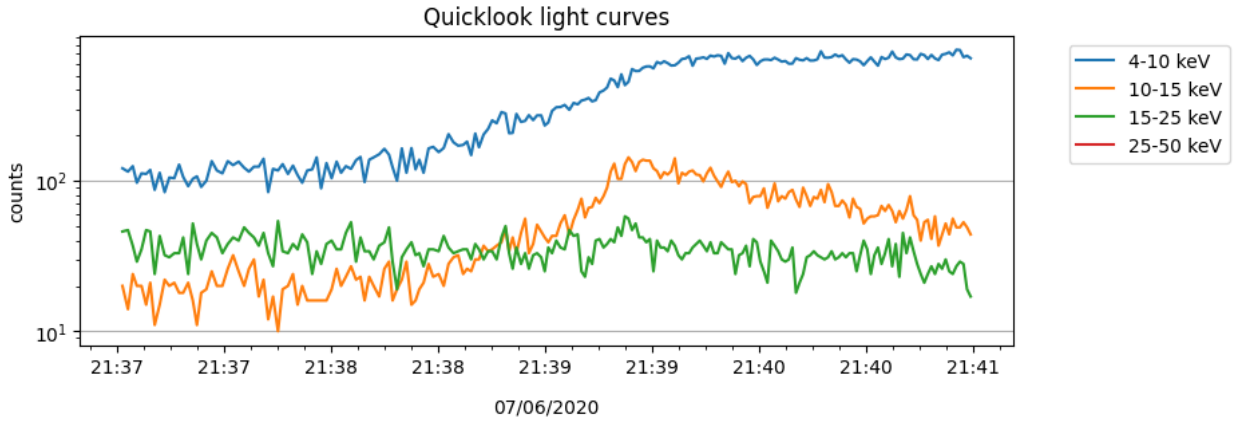

Figure 1: Quick look plot for the solar flare event on June 07, 2020 in the interval 21:37 to 21:41.

It is important mentioning that the 4-10 KeV band is affected by thermal emissions, but not all the counts come from low energy photons. The interaction with STIX instrumentation makes some higher energy photons to be attenuated such that they are detected in these lower energy bands. This reminds of the relevance of knowing the response of the detector and the detector efficiency in different energy regimes, more specifically the non diagonal terms of the response matrix that affect these low energy bands.[1]

Thermal emissions are observed to be higher at early stages of the flare evolution when the plasma reaches the highest temperatures, and its flux decay slowly. On the other hand the non-thermal emissions decay faster and are most frequently observed during the impulsive flare phase.

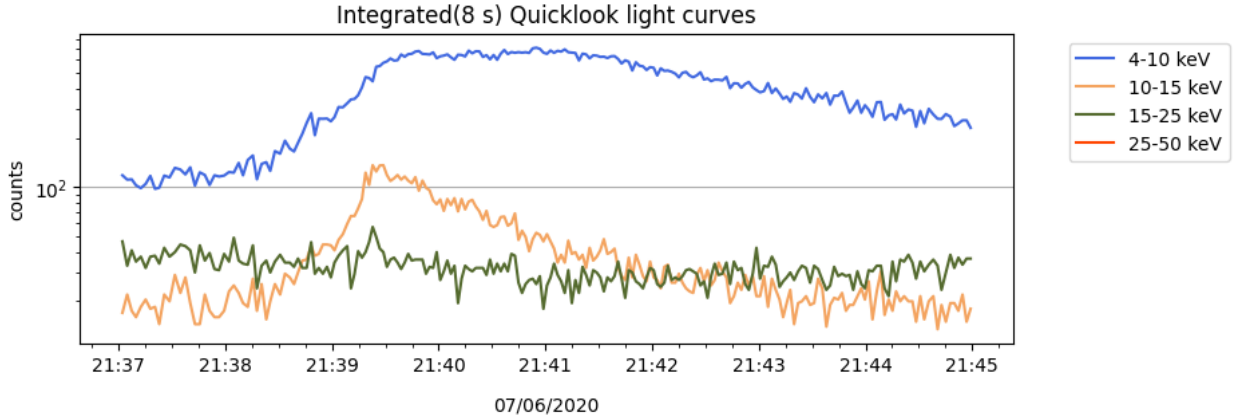

Figure 2: Integrated count signal for the same time interval and energy bands as Figure 1. The integration time is 8 seconds.

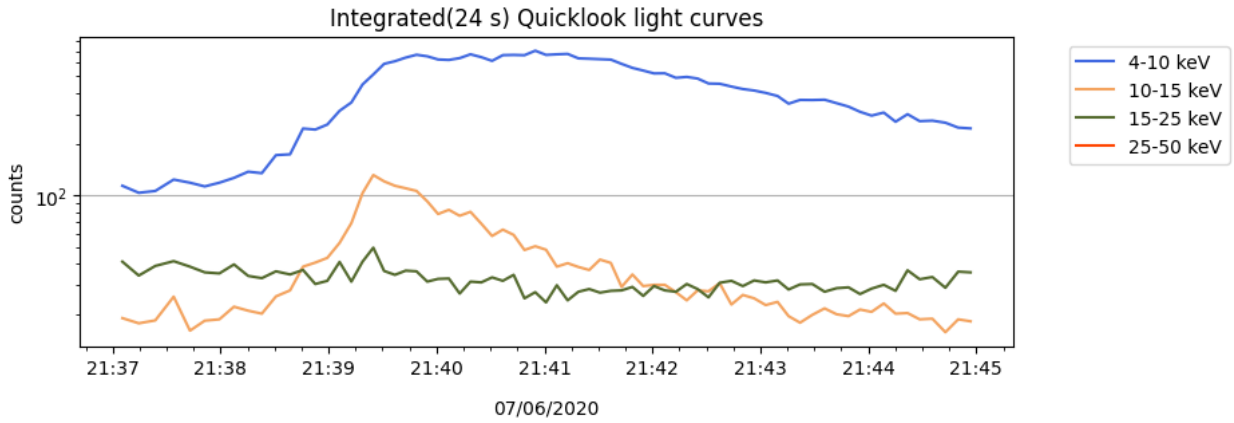

Figure 3: Integrated count signal for the same time interval and energy bands as Figure 1. The integration time is 24 seconds.

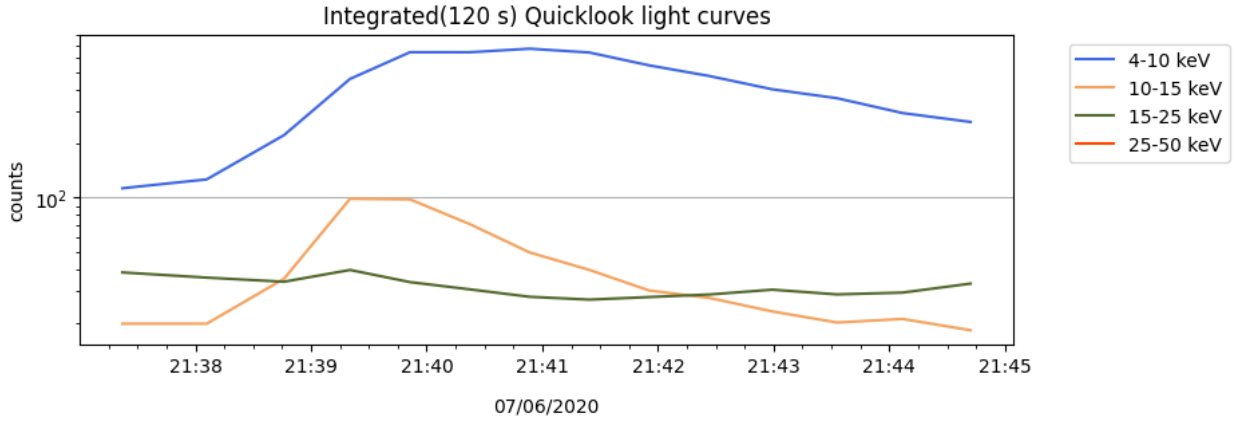

Figure 4: Integrated count signal for the same time interval and energy bands as Figure 1. The integration time is 120 seconds.

In figures 2,3 and 4 we can observe the integration of the counts overt time intervals of 8, 24 and 120 seconds respectively. Doing this we expect to suppress the effect of fluctuations in the raw signal in scales smaller than the integration time, thus smoothing the count values evolution in time and increasing the S/N ratio for some events that are clouded by fluctuations at short[1] timescales. Using integration times higher than a minute is useful for determining the trend of events of a relatively long duration, but in the case of this micro-flare we can observe that some relevant information can be lost when the event timescale is comparable to the integration time. For instance, the peak of the channel 10-15 KeV is cropped at 10^2 counts by the 120s integration time, while at shorter integration times the peak is more prominent and the peak max value is more accurate.

2 Comparison of the count rates for different detectors

STIX counts with 32 detectors, 2 of which are used for calibration. The other 30 are conveniently combining different orientations (separated by 60 degrees) and angular resolutions (10 scales) to obtain as much information of the spatial features of the solar flare events[2]. The time evolution of the counts per detector during the event is displayed in Figure 5 in the range 6 KeV to 10 KeV, and as we can see the responses are not similar in all the cases. This is expected since the detectors are build to have higher responses in scales of the order of the fringe pattern width, and towards different orientations. In fact, this different profiles are used to reconstruct the spatial information of the flare since the STIX detectors loses this information by

[1] Short relative to the integration time chosen

acting as *bucket detectors*.

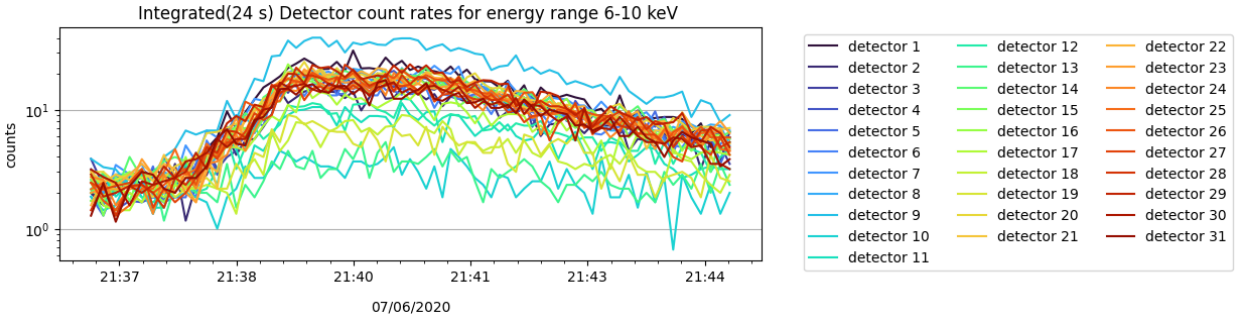

Figure 5: Integrated count signal per detector for the same time interval as Figure 1 and in the energy range 6 KeV to 10 KeV . The integration time is 24 seconds.

When grouping and summing the contributions of the detectors in each one of the 10 Sub-Collimators (SC), the different length scales are contrasted using more information (combining the counts of 3 detectors for each collimator) but the rotation information is lost. The result of this process can be seen in figure 6 and we can observe that for this event different scales had indeed different responses. For instance, SC 1 and 2 had the lowest responses, which correspond to angular resolutions between 0 and 11 arcsec. Detector 10 tracks the background signal and detector 9 is used for locating the solar flares.

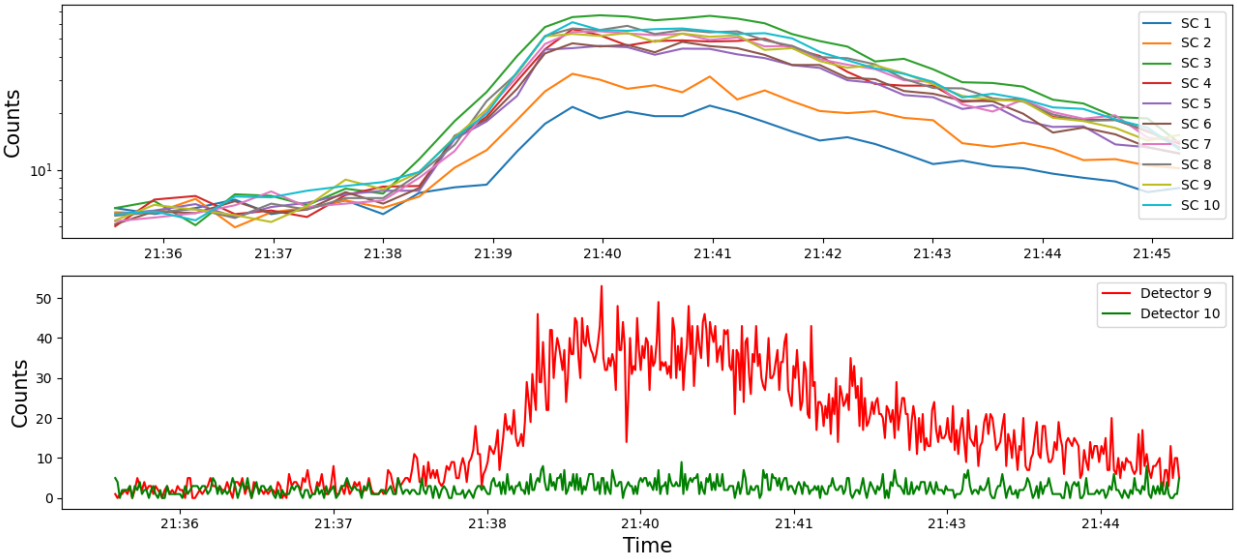

Figure 6: *Top panel:* Detectors sensible to the same length scale are grouped into subcollimators and their contributions in counts are summed. *Bottom panel:* Counts from the callibration detectors 9 (CLF) and 10 (BKG).

3 Comparison of the count rates for different pixels

Now for the same energy range (6 KeV to 10 KeV) let's see the response of the pixels in SC 10, corresponding to detectors 3,20 and 22 and a length scale of 178.6 arcsec. Let's remember that each detector is made of 4 regions each one with 3 pixels, two big ones of 9.6 mm^2 and a small one in the middle with just 1.0 mm^2. This small pixel is used to determine the presence of pulse pileup[2] in the detection by comparing its counts

[2]The detector counts the events by charge-collection in the pixels for a given integration time, under the assumption that not many photons arrive to a pixel within an integration time interval. Multiple photons interacting with the detector in a time shorter than this might corrupt the results, but its influence is not expected to be so relevant in STIX.

with the one observed in the big pixels. As we can observe in Figure 7, the smaller pixels corresponding to pixels 8, 9, 10 and 11 have less counts, which is natural given its smaller area compared to the other pixels. The increase in counts is coincident in time for both types of pixels.

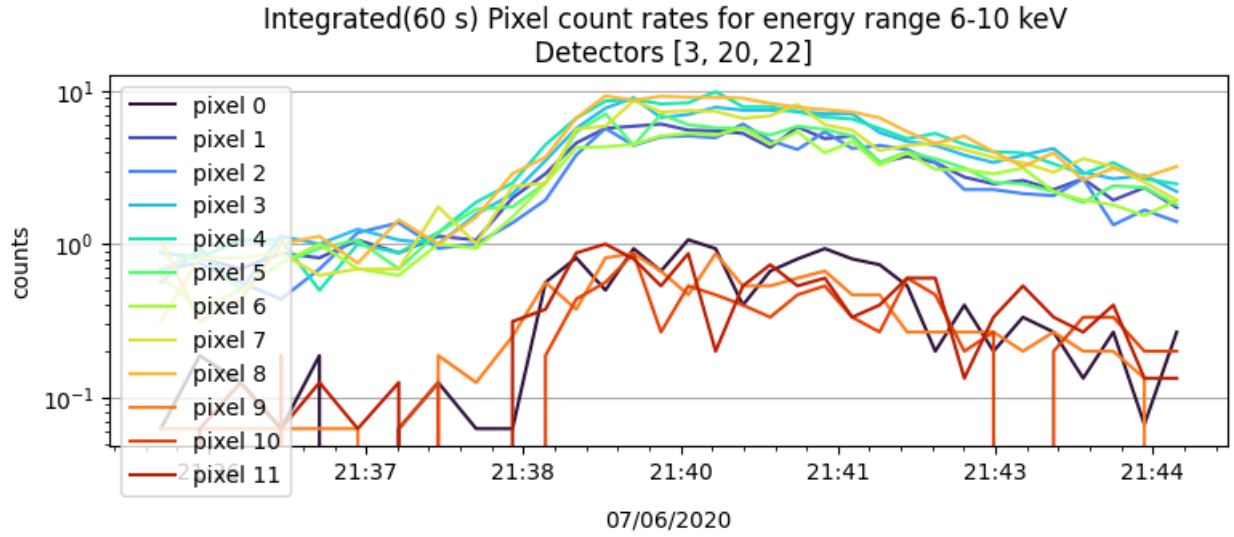

Figure 7: counts per pixel summed over detectors 3, 20 and 22 (corresponding to SC 10) for the energy interval from 6 KeV to 10 KeV. The two main groups formed correspond to the small pixels (4 lower curves) and big pixels.

4 Spectroscopy

For determining the background noise, or signal that is not coming from the flare event, I used the interval from 21h36m to 21h38m. A spectrogram is built displaying the background spectrum and the spectra for 2 different intervals: the first one from 21h38m59s to 21h39m19s (displayed in figure 8) and the second from 21h40m39s to 21h40m59s (displayed in figure 9). For each case the flare spectrum is obtained by subtracting the background spectrum from the flare observations. The Spectral index is then estimated by doing a power law fit over the tail of the distribution.

In the first case we observe a spectral index of $\gamma = 5.24$ consistent with the one reported by Battaglia et al. [1] ($\gamma = 5.6 \pm 0.3$) for non-thermal processes, thus confirming that for energy bands above 10 KeV most of the counts correspond to non-thermal processes.On the other hand, the second case correspond to the thermal peak for which the non thermal emissions decayed thus corresponding to higher a spectral index $\gamma = 7.61$. This value is close the range reported by the publication ($\gamma = 7.0 \pm 0.5$) for non thermal electrons.

References

[1] A. F. Battaglia, J. Saqri, P. Massa, E. Perracchione, E. C. M. Dickson, H. Xiao, A. M. Veronig, A. Warmuth, M. Battaglia, G. J. Hurford, A. Meuris, O. Limousin, L. Etesi, S. A. Maloney, R. A. Schwartz, M. Kuhar, F. Schuller, V. Senthamizh Pavai, S. Musset, D. F. Ryan, L. Kleint, M. Piana, A. M. Massone, F. Benvenuto, J. Sylwester, M. Litwicka, M. Stęślicki, T. Mrozek, N. Vilmer, F. Fárník, J. Kašparová, G. Mann, P. T. Gallagher, B. R. Dennis, A. Csillaghy, A. O. Benz, and S. Krucker, "STIX X-ray microflare observations during the Solar Orbiter commissioning phase," , vol. 656, p. A4, Dec. 2021.

[2] S. Krucker, G. J. Hurford, O. Grimm, S. Kögl, H. P. Gröbelbauer, L. Etesi, and et al., "The Spectrometer/Telescope for Imaging X-rays (STIX)," , vol. 642, p. A15, Oct. 2020.

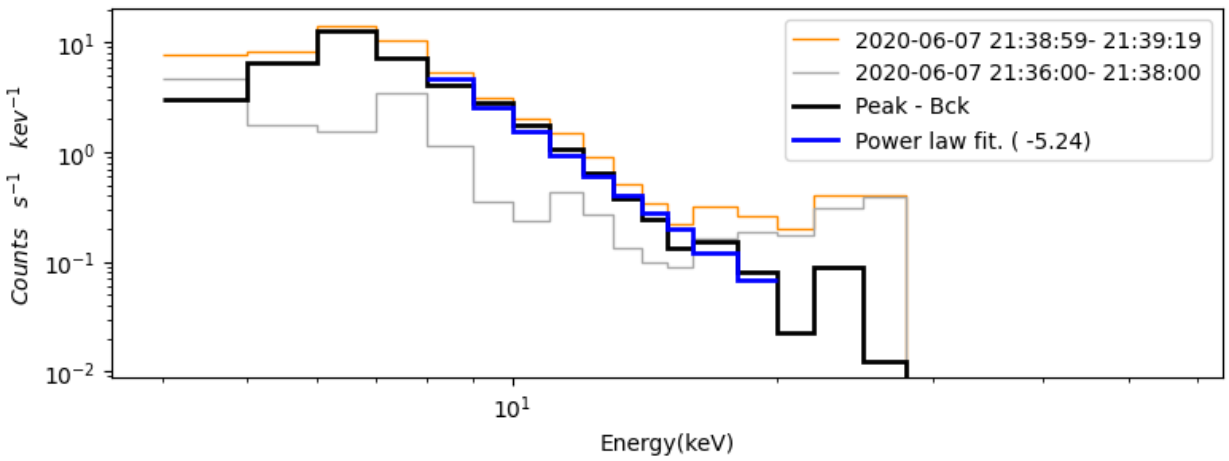

Figure 8: Spectrogram containing the background spectra (for the time interval from 21h36m to 21h38m) and the peak spectra in the interval 21h38m59s to 21h39m19s. The subtraction result in the clean peak spectra in which a linear fit is done, obtaining an spectral index of $\gamma = 5.24$.

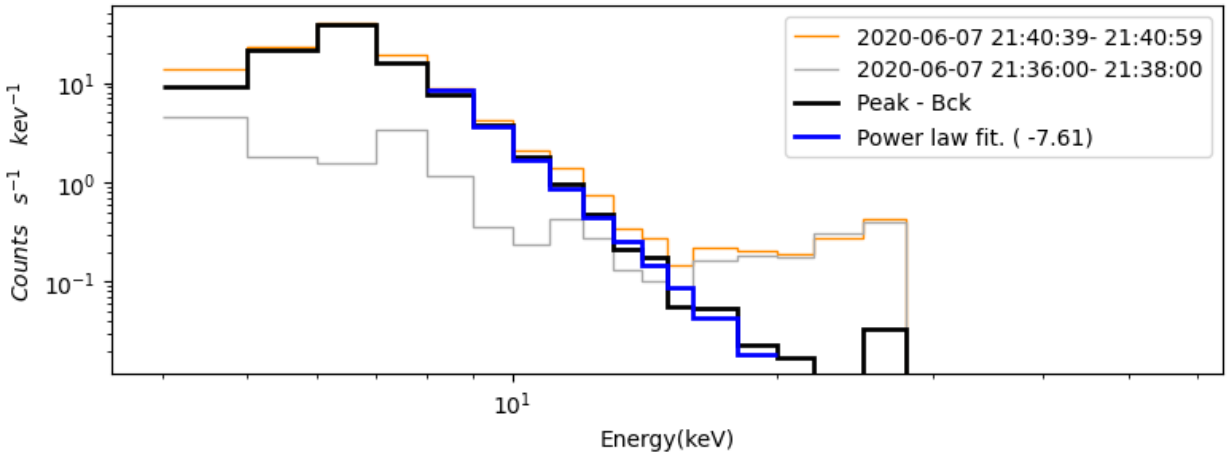

Figure 9: Spectrogram containing the background spectra (for the time interval from 21h36m to 21h38m) and the peak spectra in the interval 21h40m39s to 21h40m59s. The subtraction result in the clean peak spectra in which a linear fit is done, obtaining an spectral index of $\gamma = 7.61$.